ELSEVIER

Ultramicroscopy 74 (1998) 61–73

ultramicroscopy

Towards quantitative electron holography of magnetic thin films using in situ magnetization reversal

R.E. Dunin-Borkowski[a,*], M.R. McCartney[a], David J. Smith[a,1], S.S.P. Parkin[b]

[a] *Center for Solid State Science, Arizona State University, Tempe, AZ 85287-1704, USA*
[b] *IBM Almaden Research Center, 650 Harry Road, San Jose, CA 95120-6099, USA*

Received 17 November 1997; received in revised form 23 February 1998

Abstract

An approach based on off-axis electron holography has been developed for quantifying the magnetization in a sample of unknown local thickness with lateral variations in composition. The magnetic field of the objective lens is used to reverse the magnetization direction in the sample without altering its magnitude, thereby enabling phase changes due to magnetization to be separated from those due to thickness and compositional variations. The technique is demonstrated in applications to a lithographically patterned magnetic film on a silicon nitride membrane and a cross-sectional sample containing a magnetic tunnel junction. The importance of dynamical diffraction effects and fringing fields is discussed.

Keywords: Off-axis electron halography; Magnetic thin films; In situ magnetization reversal

1. Introduction

An off-axis electron hologram obtained in a transmission electron microscope (TEM) can, in principle, be used to determine the magnitude and direction of the in-plane magnetization within a magnetic material to nanometer resolution [1]. In practice however, the phase of the recorded holographic interference fringes is almost always complicated by the presence of local variations in the mean inner potential and/or the thickness of the sample. These factors also affect methods for determining magnetization based on differential phase contrast [2–5]. Most electron holographic studies of magnetic materials have thus either been qualitative or else some knowledge (or at least an estimate) of the specimen thickness profile has been required [6–8].

Magnetic materials of current interest contain both magnetic and non-magnetic regions, and their compositions are likely to vary on the nanometer scale [9]. A technique for magnetization characterization is thus required that does not rely on knowledge of the local specimen thickness, which may also vary in a complicated manner. In this paper,

* Corresponding author.
[1] Also at: Department of Physics and Astronomy, Arizona State University, Tempe, AZ 85287-1504, USA.

0304-3991/98/$19.00
PII: S0304-3991(98)00023-0

we describe a new approach based on off-axis electron holography, which allows both mean inner potential and specimen thickness effects to be separated from the recorded phase, enabling the magnetization to be extracted. The approach involves the analysis of two successive holograms, where the magnetization direction in the sample has been reversed in situ using the magnetic field of the objective lens.[2] An obvious requirement is that complete reversal of the magnetization can be achieved, which in turn will depend upon the shape anisotropy of the sample.

We begin by illustrating the basic procedure for removing mean inner potential contributions from the phase through the characterization of a magnetic film lithographically patterned on a silicon nitride membrane. The further removal of specimen thickness effects from a measured magnetization profile is then demonstrated through the analysis of a cross-sectional sample containing a magnetic tunnel junction.

2. Experimental details

Experimental off-axis electron holograms were recorded at 200 kV using a Philips CM200 TEM equipped with a field emission gun, an electrostatic biprism and a 1024×1024 pixel Gatan 794 multiscan CCD camera. Reference holograms were used to exclude artifacts associated with local irregularities of the image/recording system [11], but point-spread-function deconvolution was not applied since it would increase the noise in the holographic interference fringes without altering their phase substantially. A Lorentz mini-lens ($C_S = 8$ m and 1.2 nm line resolution at 200 kV) situated below the lower objective polepiece allowed holograms to be obtained with the objective lens switched off so that the sample was in almost field-free conditions (the residual magnetic field in the beam direction was then ~ 0.015 T). Samples were tilted by $\pm 30^\circ$ from the horizontal in order to magnetize them in situ using the conventional objective lens, with the component of the applied field in the specimen plane suitably chosen to exceed the coercive field of the layers of interest. It was assumed that the resulting magnetization was solely in-plane [12]. Fig. 1 shows the Hall probe calibration of the field as a function of objective lens current. (The objective lens is switched off when the lens reading is ~ 5 mA). The residual field of ~ 0.015 T at the specimen plane was unaffected by the excitation of the Lorentz lens, although the value at the level of the lower objective lens pole-piece increased slightly with lens current.

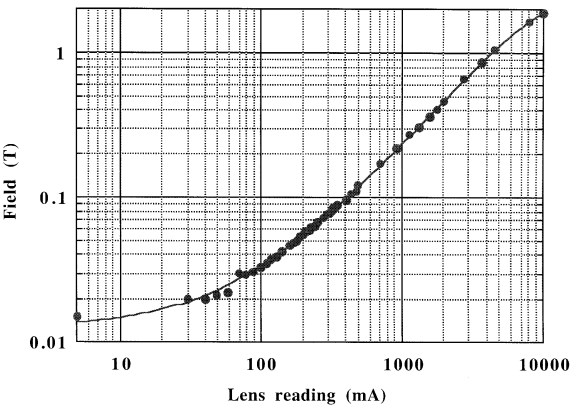

Fig. 1. Hall probe measurements of magnetic field in specimen plane of Philips CM200 as function of objective lens current. Field is parallel to incident beam direction and is insensitive to changes in specimen height.

3. Off-axis electron holography of patterned magnetic thin film on silicon nitride window

The first specimen examined was a patterned test structure grown on a silicon nitride window. Our specific interest was to develop a technique that would be suitable for characterizing the magnetic coupling between microstructured magnetic tunnel junctions that exhibit shape anisotropy-controlled magnetoresistive behavior [13,14]. The specimen was made by depositing a cobalt film of 30 nm nominal thickness onto a 50 nm thick silicon nitride membrane with patterning into three 300 nm long letters using standard electron-beam

[2] For many samples, in situ magnetization reversal is both more appropriate and more convenient than removing the sample from the microscope and turning it upside down before recording the second hologram [1,10].

lithography and lift-off procedures. The nominal thickness of 30 nm was chosen since this value was of the same order as the thickness of the tunnel junctions of interest. The resulting phase shifts should also change slowly enough to allow successful phase unwrapping of the hologram. Previous work on similar patterned magnetic films [15] involved the study of domains *within* individual structures, but little work has yet been published on the magnetic interactions *between* patterned shapes [16].

Fig. 2 shows one of a pair of experimental off-axis electron holograms, which were obtained after magnetizing the cobalt film by applying fields parallel, and antiparallel, to the vertical strokes of the letter "U". Qualitatively, the holograms appeared identical, irrespective of the direction of magnetization. The biprism voltage was 100 V, corresponding to an overlap region at the sample of width 600 nm, and the sampling density of the image was 1.5 nm/pixel. The holographic fringe contrast, as defined by the expression

$$\mu = \left(\frac{\max - \min}{\max + \min}\right), \tag{1}$$

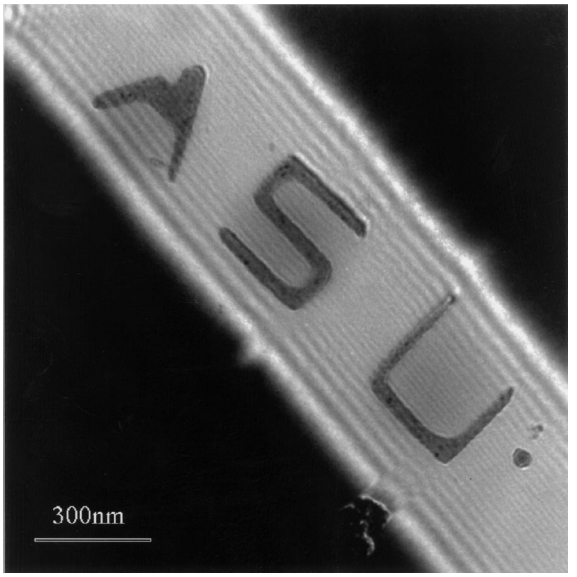

Fig. 2. Electron hologram of cobalt letters of nominal thickness 30 nm patterned onto silicon nitride film using electron beam lithography. Letters were magnetized by applying field in situ parallel and antiparallel to vertical strokes of "U". Accelerating voltage was 200 kV and biprism voltage was 100 V. Black = 950 and white = 1500 counts.

where max and min refer to the intensity of the fringes in the silicon nitride film, was approximately 0.5%. This value for the contrast was much lower than normally used for holographic reconstruction both because the reference wave passed through the silicon nitride membrane and because low magnification (resulting in a sampling density of only 3.4 pixels per holographic fringe) was required to include all three letters in a single hologram.

In the absence of dynamical diffraction and Fresnel contrast effects, the phase of the holographic fringes is given (in one dimension) by

$$\phi(x) = C_{\mathrm{E}} \int V(x, z)\, \mathrm{d}z - \left(\frac{e}{\hbar}\right) \iint B_{\|}(x, z)\, \mathrm{d}x\, \mathrm{d}z, \tag{2}$$

where z is the incident beam direction, x is a direction that lies in the plane of the sample, V is the mean inner potential and $B_{\|}$ is the component of the magnetic field perpendicular to both x and z. The constant C_{E} is given by

$$C_{\mathrm{E}} = \left(\frac{2\pi}{\lambda}\right)\left(\frac{E + E_0}{E(E + 2E_0)}\right), \tag{3}$$

where λ is the wavelength, E is the kinetic energy and E_0 is the rest mass energy of the incident electron. If neither V nor $B_{\|}$ vary with z (as would be the case for a cross-sectional sample, in the absence of surface contamination layers and fringing fields), then

$$\phi(x) = C_{\mathrm{E}} V(x) t(x) - \left(\frac{e}{\hbar}\right) \int B_{\|}(x) t(x)\, \mathrm{d}x \tag{4}$$

and

$$\frac{\mathrm{d}\phi(x)}{\mathrm{d}x} = C_{\mathrm{E}} \frac{\mathrm{d}}{\mathrm{d}x} \{V(x) t(x)\} - \left(\frac{e}{\hbar}\right) B_{\|}(x) t(x). \tag{5}$$

Eqs. (4) and (5) demonstrate the fact that the in-plane magnetization would be proportional to the gradient of the phase *in a sample of uniform thickness and composition.*

In most magnetic samples, the mean inner potential term $V(x)t(x)$ dominates both the phase and the phase gradient, complicating attempts to quantify the magnetization. This is the case in Fig. 3a, which shows the unwrapped phase calculated from an

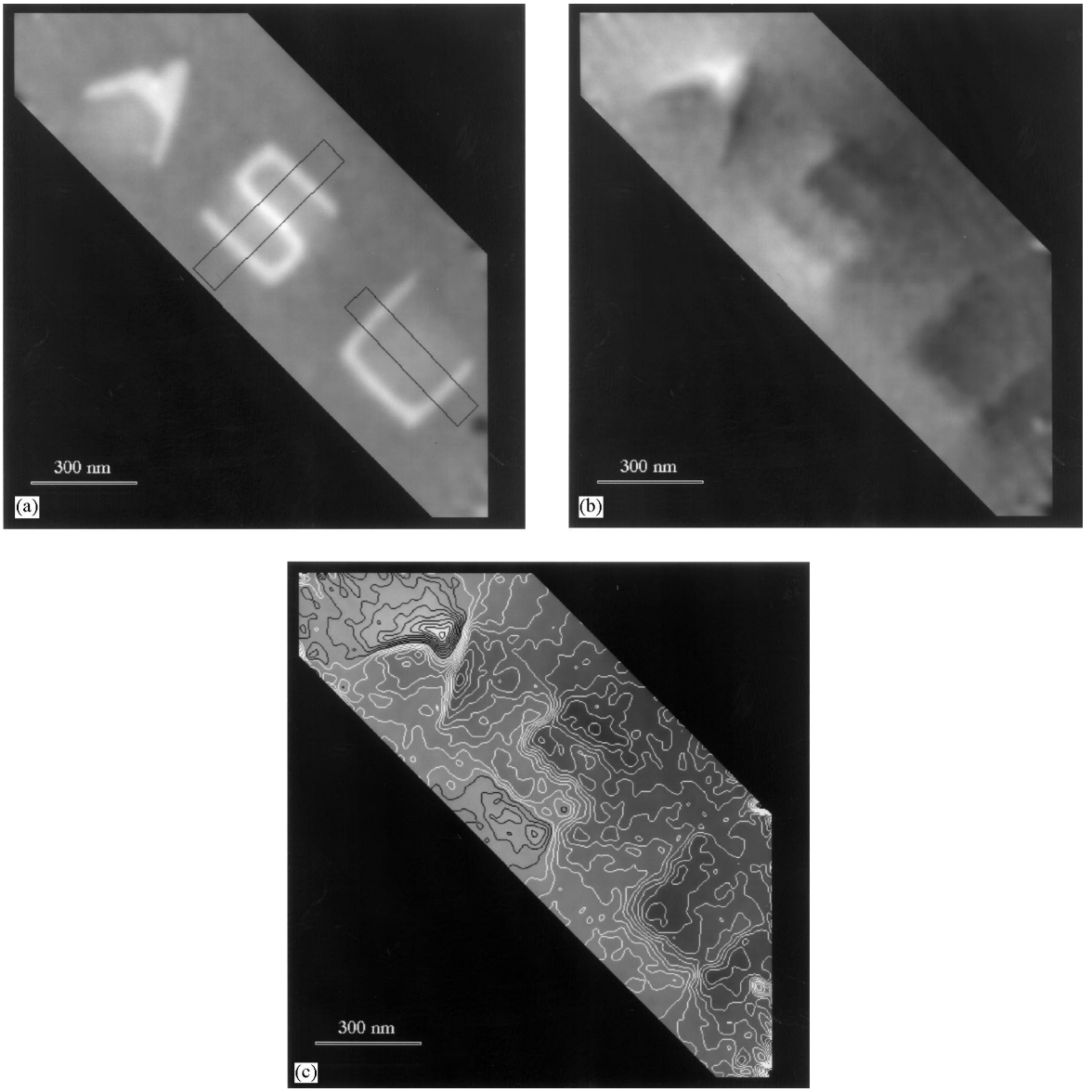

Fig. 3. (a) Unwrapped phase from individual hologram of patterned letters (black = 0 and white = 9 radians). Two regions chosen for subsequent analysis are marked. (b) Phase difference between holograms obtained with letters magnetized parallel and antiparallel to vertical strokes of "U" (black = 0 and white = 9.7 radians). (c) 30 contours, equally spaced between values of 0 and 12 radians, added to phase difference image shown in (b).

individual hologram of the patterned cobalt letters using a sideband of size 128×128 pixels [11]. (The dark contrast exhibited by the dot to the right of the letter "U" indicates that it originates from the reference wave.) The phase in Fig. 3a is dominated by the mean inner potential contribution associated with the presence of cobalt.

Examination of Eq. (2) indicates that a *difference* between the phases of two holograms where only the magnetization has been reversed would remove

the dominant mean inner potential contribution and provide exactly twice the magnetic contribution to the phase. This procedure has been applied to a pair of holograms of the cobalt letters, as shown in Fig. 3b. All mean inner potential (and electrostatic fringing field) effects have now been removed and only the magnetic contribution to the phase remains. The magnetic fringing fields between the letters are particularly striking in Fig. 3c, which shows phase contour lines overlaid at 30 equal intervals over a range of 12 radians. Domain walls are visible in the letters at the bottom right corners of the "S" and the "U" and at the top left corner of the "S". The positions of these walls were shown from the separate phase images to remain unchanged after the magnetization was reversed. (The domain wall in the "U" is required because the vertical strokes were magnetized in the same direction). The greatest fringing field originates from a small notch in the letter "A".

Quantitative measurements of the magnetization may be made from Fig. 3b, although the results must be interpreted with care for this specimen because of the presence of magnetic fringing fields above and below the film as well as in its plane. The line profiles in Fig. 4 correspond to the regions marked in Fig. 3a, and show the average phase obtained from the two holograms (i.e. only the mean inner potential contribution to the phase), and half of the difference between the phases (i.e. only the magnetic contribution to the phase). The average phase does not drop to the value of the silicon nitride between the bars of the letters, most likely due to the presence of residual material from the lithography processing.

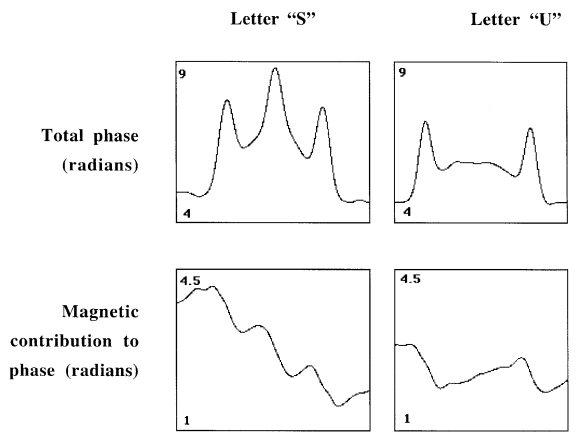

Fig. 4. Line traces from regions shown in Fig. 3a. Total phase is average of phases obtained from holograms with letters magnetized parallel and antiparallel to vertical strokes of "U". Magnetic contribution is half of difference between phases.

Application of Eq. (4) to the phase profiles in Fig. 4 (using a value of 29.5 V for the mean inner potential of cobalt, calculated using the neutral atom scattering factors of Rez et al. [17]) suggests that the true cobalt film thickness ranged from 10 to 20 nm. If Eq. (5) is applied directly to the gradients of the magnetic contribution to the phase, then values for the magnetization within each letter of between 0.6 and 1.4 T are obtained even after thickness variations are taken into account. (The value for pure cobalt is expected to be 1.76 T [18]). The lower and higher values correspond to the bars in the "S" and the "U", respectively. The difference between the values measured for the "S" and the "U" must result from different demagnetizing fields associated with the complicated specimen geometry. The range of magnetization values obtained here should not be taken as an indication of the precision of the technique. Applications to patterned Co nanostructures of simpler geometry have since confirmed the ability to obtain reproducible and quantitative results [19].

The magnetic fringing field in the regions *between* the letters may be quantified, although it should be appreciated that only a projection in the incident beam direction is recorded whereas the fringing field varies in three dimensions. The magnitude of the fringing field between different regions of the sample may, however, be compared. For example, if it were assumed for illustrative purposes that the fringing field took a single value in the beam direction within a slab of thickness 15 nm (this is the average value of the measured cobalt film thickness), then its measured values between the bars of the "S" and the "U" would be 0.20 and 0.15 T respectively.

The above example has demonstrated the basic procedure for removing the contributions of the mean inner potential from the phase of a hologram from a magnetic material. However, a two-dimensional map such as that shown in Fig. 3c is not very

useful for a cross-sectional sample containing a magnetic thin film or multilayer, since contours of constant magnetization then simply lie parallel to the magnetic layers. Quantitative measurements of the magnetization may also be complicated by the presence of unknown and rapid variations in the sample thickness associated with local changes in composition. These problems will now be addressed.

4. Off-axis electron holography of a cross section containing several magnetic layers

The cross-sectional sample chosen for analysis was a polycrystalline tunnel junction grown on [0 0 1] Si by DC sputtering. The layer sequence comprised nominally 500 nm SiO_2|25 nm $Cr_{0.8}V_{0.2}$| 15 nm $Co_{0.75}Pt_{0.12}Cr_{0.13}$|1.4 nm AlO_x|15 nm $Co_{0.88}Pt_{0.12}$|20 nm Al, with the AlO_x layer acting as the tunnel barrier. The CoPtCr and the CoPt are hard and soft ferromagnetic layers with coercive fields of ~ 0.3 and ~ 0.02 T, respectively. From Fig. 1, it can be concluded that the objective lens can be used to reverse either the magnetizations of both layers together or that of the soft magnetic layer alone. (For example, at a tilt angle of 30°, applied fields of greater than 0.6 and 0.04 T are required to reverse the magnetizations of the layers, corresponding to objective lens currents of 2500 and 135 mA). The magnetizations of the hard and soft layers are expected to be approximately 0.5 and 1.5 T, respectively.

4.1. Removal of specimen thickness effects for magnetization characterization

The important point that magnetic contributions to the phase and the phase gradient are much smaller than any contributions from changes in mean inner potential in a cross-sectional sample is demonstrated by the simulations shown in Fig. 5. Eqs. (4) and (5) were used to calculate phase and phase gradient profiles for the present cross-sectional tunnel junction sample, assuming a representative parabolic thickness profile (shown in Fig. 5a). Values of 17, 30, 18, 30, 28 and 10 V (calculated using the neutral atom scattering factors of Rez et al. [17]) were used for the mean inner potentials of Al, CoPt, AlO_x, CoPtCr, CrV and SiO_2 respectively (Fig. 5b), and for illustrative purposes magnetizations of 2 T (Fig. 5e and Fig. 5j) were assigned to both the CoPtCr and the CoPt layers. The magnetizations of both the CoPtCr and the CoPt layers were reversed between Fig. 5e–Fig. 5i and Fig. 5j–Fig. 5n, and no fringing field or dynamical diffraction effects were included in the simulations.

The large difference between the magnetic and mean inner potential contributions to the phase and phase gradient is apparent from a comparison of figures such as Fig. 5g and Fig. 5i. It is also particularly interesting to observe the similarity between the shapes of the magnetization profiles (Fig. 5e and Fig. 5j) and the magnetic contributions to the phase gradient (Fig. 5g and Fig. 5l). This similarity suggested the possibility that differences in the phase *gradient* between images in which the magnetization has been reversed could provide the basis for more accurate magnetization characterization. In contrast, the magnetic contributions to the phase (Fig. 5f and Fig. 5k) change cumulatively across an image. Differences between phase profiles (Fig. 5h and Fig. 5m) could therefore be used to determine *whether* changes in magnetization have taken place between two holograms.

The magnetization profiles (Fig. 5e and Fig. 5j) differ from the magnetic contributions to the phase gradient (Fig. 5g and Fig. 5l) only because of variations in specimen thickness within the magnetic layers. We now consider how contributions due to specimen thickness can be eliminated in order to characterize the magnetization more accurately.

Rearrangement of Eqs. (4) and (5) for two successive holograms indicates that the specimen thickness may be removed[3] by plotting the difference in the phase gradient between images in which the magnetization has reversed divided by the average of their phases, multiplied by a constant and

[3] The determination [20] of the local specimen thickness from the normalized amplitude of a hologram A_n using the relation $t = -2\lambda \ln(A_n)$ is not viable here both because the value of λ in each material in such a cross-sectional sample is generally not known, and also because the amplitude image is much noisier than the phase image and contains correspondingly greater contributions from diffraction and Fresnel contrast.

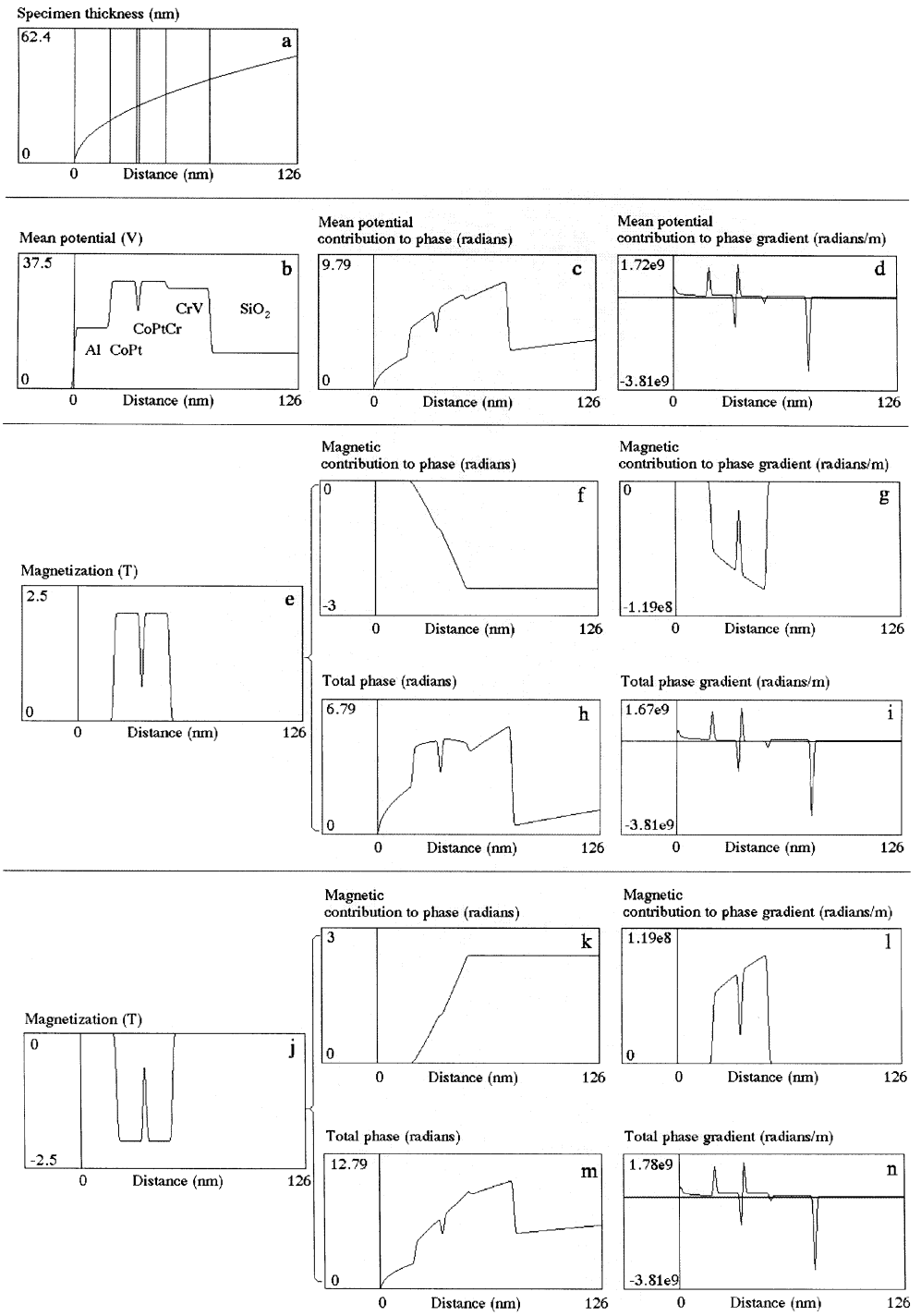

Fig. 5. One-dimensional calculations of phase and phase gradient for tunnel junction examined in cross section, for representative parabolic specimen thickness profile. For illustrative purposes, magnetizations of 2 T have been assigned to CoPtCr and CoPt layers, and values of 17, 30, 18, 30, 28 and 10 V assigned to mean inner potentials of Al, CoPt, AlO_x, CoPtCr, CrV and SiO_2, respectively. Dynamical diffraction effects have not been included. (c–d) show only mean inner potential contributions to phase and phase gradient. Magnetization is reversed between (e–i) and (j–n).

by the value of the mean inner potential of each magnetic layer separately. Formally, this process is written as

$$\left(\frac{C_E \hbar V(x)}{e}\right)\left\{\frac{\Delta[\mathrm{d}\phi(x)/\mathrm{d}x]}{\langle\phi(x)\rangle}\right\} \equiv \frac{\Delta[B_{\|}(x)]}{(1-(e/C_E\hbar V(x))\{\langle\int B_{\|}(x)t(x)\,\mathrm{d}x\rangle/t(x)\}\rangle}. \quad (6)$$

Although this expression looks complicated initially, what it means is that by combining the phase profiles and phase gradients from successive holograms in which the magnetization direction has been reversed, the specimen thickness profile is eliminated and the magnetization can be determined quantitatively. This process is equivalent to using the average phase to calculate the specimen thickness and then using this knowledge to eliminate the thickness from the magnetic contribution to the phase gradient. Most importantly, analysis reveals that both the magnitude and the sign of $\Delta[B_{\|}(x)] \equiv 2B_{\|}(x)$ are obtained *exactly* using Eq. (6) if the magnetization reverses everywhere while maintaining its magnitude (the denominator on the right-hand side of the equation is then unity). Furthermore, non-zero values are returned only in regions where the magnetization has changed.

Fig. 6 illustrates the application of Eq. (6) to the simulations in Fig. 5. It can be concluded that only a cumulative effect of variations in magnetization would be visible in the difference between the simulated phases (Fig. 5h and Fig. 5m). The difference between the phase gradients (Fig. 6b) would be more representative of the true magnetization profile. In contrast, Fig. 6c shows that, when Eq. (6) is applied to the simulated profiles, the original magnetization profile is returned exactly, with all effects associated with variations in specimen thickness removed. The uncertainty in the inferred magnetization will be directly proportional to the accuracy to which the mean inner potential is known.

4.2. Application to experimental holograms

Fig. 7 shows a typical off-axis electron hologram obtained from a cross-sectional sample of the tunnel junction, at a sampling density of 0.34 nm/pixel. The biprism voltage was 90 V, corresponding to an overlap region of width 510 nm. The high magnification

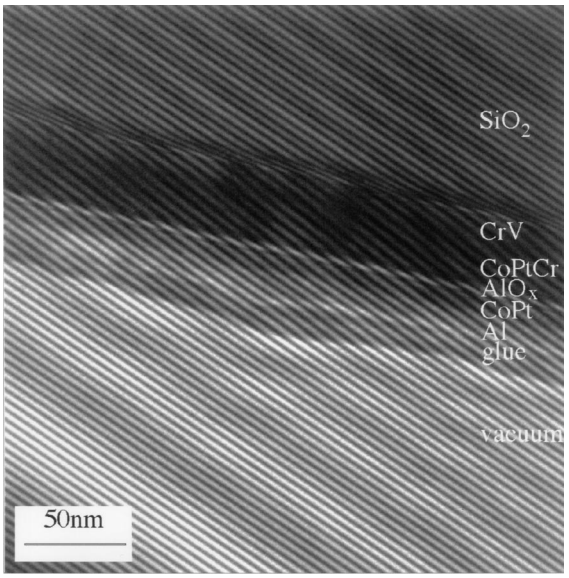

Fig. 7. Representative electron hologram obtained from long, straight and unbroken region of magnetic tunnel junction examined in cross-section, using accelerating voltage of 200 kV and biprism voltage of 90 V. Black = 75 and white = 250 counts.

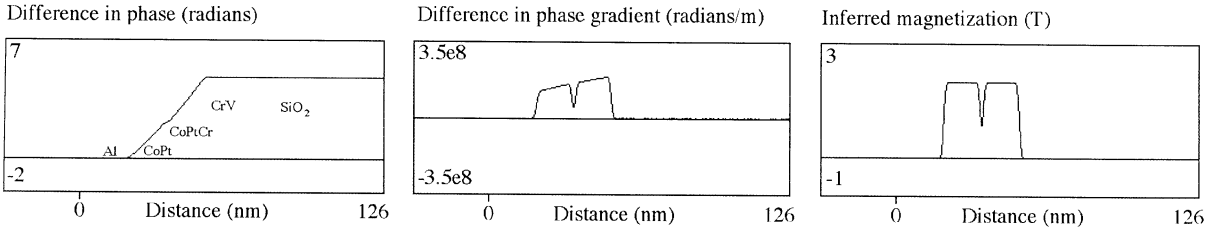

Fig. 6. Difference between phases, difference between phase gradients and inferred magnetization from simulations for different magnetization directions in Fig. 5.

used in recording the hologram resulted in a sampling density of 14.9 pixels per interference fringe, and the interference fringe contrast was approximately 28% (using the definition of Eq. (1)).

Similar to the results for the patterned cobalt film, the holograms appeared identical irrespective of the direction of magnetization of the layers. However, differences became immediately apparent in the unwrapped phase. This was determined using a sideband of size 256×256 pixels [11], as shown in Fig. 8a. Both the magnitude and the gradient of the phase in vacuum have been scaled to zero in the profiles. Similar to the simulations in Fig. 5, the changes in magnetization (in this case in both the hard and the soft layers) are manifested as a clear difference in the phase of the SiO_2 with respect to the vacuum. Fig. 8b shows the difference between the phases in Fig. 8a (note the similarity to the simulation in Fig. 5k). It should be clear that there are no significant magnetic fringing fields since these would have resulted in a difference between the gradient of the phase difference in the SiO_2 and the vacuum (see below). Fig. 8c shows the difference between the phase gradients, and verifies that the magnetization of the CoPtCr and the CoPt layers has indeed reversed. Finally, Fig. 8d shows the corresponding profile of $\Delta[B_{\|}(x)] \equiv 2B_{\|}(x)$, which was obtained by applying Eq. (6). This profile should now be independent of experimental variations in specimen thickness. The AlO_x barrier, of nominal thickness 1.4 nm, is clearly resolved (arrowed) in Fig. 8d. The inferred magnetizations of approximately 0.5 and 1 T for the CoPtCr and CoPt layers are of the same order as the expected magnetizations. However, it is possible that the details in Fig. 8d may be associated with Fresnel effects, which are discussed in the following section. It is important to note that the magnetization in the region of interest is almost certain to take the form of a single domain in the plane of the film, after it has been magnetized in situ, as a result of the geometry of a cross-sectional sample.

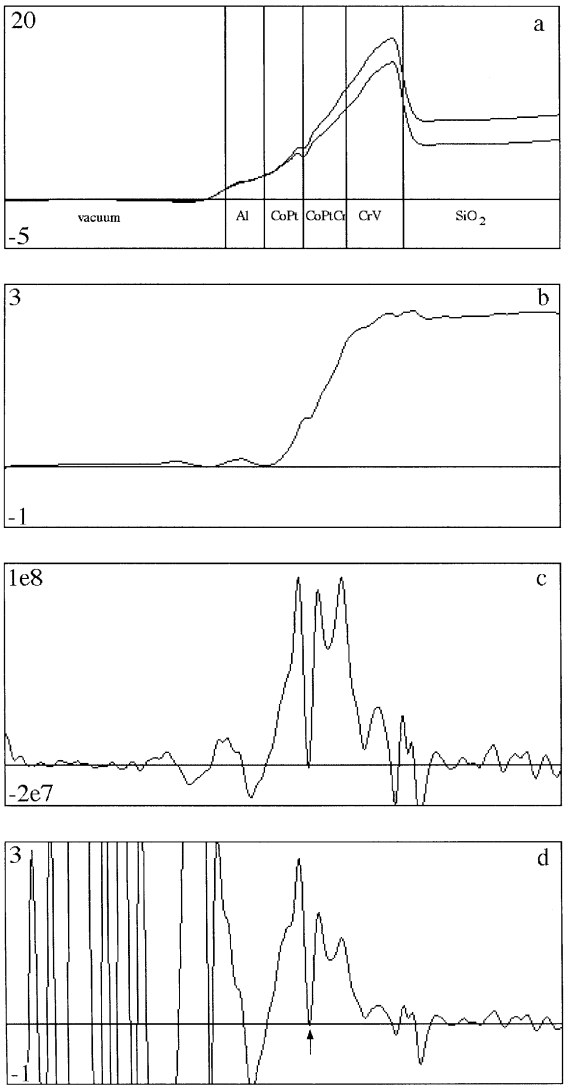

Fig. 8. (a) Experimental phases in radians with CoPt and CoPtCr magnetized parallel and antiparallel to layers, but always in same direction as each other; (b) difference between traces in (a); (c) difference between gradients of phases in radians per m; (d) $\Delta[B_{\|}(x)] \equiv 2B_{\|}(x)$ (i.e. twice inferred magnetization) in T.

4.3. Possible sources of error

The magnetic layers examined in Figs. 7 and 8 were unbroken and appeared to be uniform in cross-section along their length. Thus, the magnitude of any magnetic fringing fields [21] surrounding them was minimal. Fig. 9 shows a hologram obtained from a region of sample where the magnetic layers terminated. The phase difference between images obtained with the layers magnetized in opposite directions (Fig. 10) now exhibits

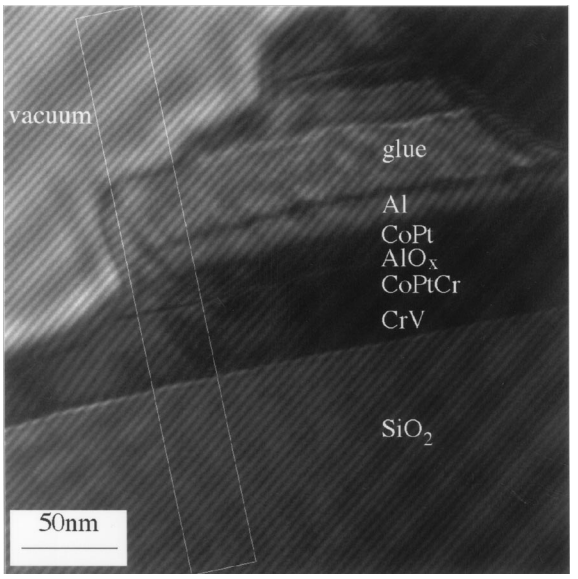

Fig. 9. Representative electron hologram obtained from region of sample where layers terminate, using accelerating voltage of 200 kV and biprism voltage of 90 V. Black = 121 and white = 433 counts. Region chosen for subsequent analysis is marked.

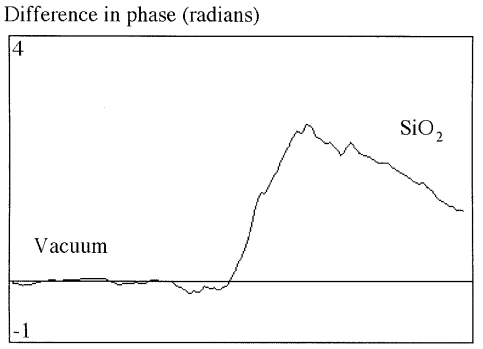

Fig. 10. Phase difference (in radians) between traces obtained from region marked in Fig. 9 for opposite magnetizations of layers, showing different gradient in vacuum on left and SiO_2 on right due to presence of fringing fields.

different gradients in the SiO_2 and the vacuum, indicating the presence of fringing fields outside the magnetic layers. In such cases, the magnetization behavior is much more difficult to interpret. Nevertheless, it should still be possible to assess whether magnetic fringing fields are significant from profiles such as that shown in Fig. 10, since the effects of any electrostatic fringing fields are automatically removed when Eq. (6) is applied.

The accuracy with which the magnitude of $B_{\|}(x)$ can be inferred using Eq. (6) is limited by the degree to which the mean inner potential of the area of interest can be estimated. However, it should be noted that the approach is not affected by contributions to the phase from diffraction contrast within each material if the local orientation of the specimen is identical for the two holograms. Experimentally, surface contamination layers should be thin in order to validate multiplication by the local value of the mean inner potential. The sample thickness should also not be too small since division by the average phase would then substantially increase noise in the inferred magnetization.

The primary disadvantage of using Eq. (6) is that it utilizes differences between subtle changes in the phase gradient. Thus, holograms of high quality are required. Moreover, a reliable phase-unwrapping procedure is needed wherever $V(x)t(x)$ changes abruptly [11]. Fig. 11 illustrates the additional artifacts that can result from a small misalignment between the phases of the two holograms. It is thus important to register the holograms to sub-pixel accuracy before calculating $B_{\|}(x)$.

A final point for consideration is the effect on the phase of Fresnel contrast associated with dynamical diffraction at each interface in a cross-sectional sample. Results of one-dimensional multislice calculations of phase for the present sample, incorporating both the electrostatic and the magnetic contributions to changes in the specimen potential, are shown in Fig. 12 for uniform specimen thicknesses of 5 and 50 nm and defoci of 0 nm (Gaussian focus) and -4479 nm (Scherzer focus). The calculations were performed for an accelerating voltage of 200 kV and a C_S of 8 m, the slice thickness and sampling density were 0.1 nm and 0.2 nm/pixel, respectively, and beam convergence had little effect on the calculated phases. The profiles in Fig. 12 exhibit additional oscillations in the phase, which were not present in the simpler calculations used for Fig. 5. However, experimentally (see above) the phase was calculated using a sideband that was four or eight times smaller than the original hologram [11]. For typical microscope magnifications, such as those used for Figs. 7 and 9, this procedure effectively filters out the higher spatial frequency Fresnel fringe effects visible in Fig. 12. Fig. 13

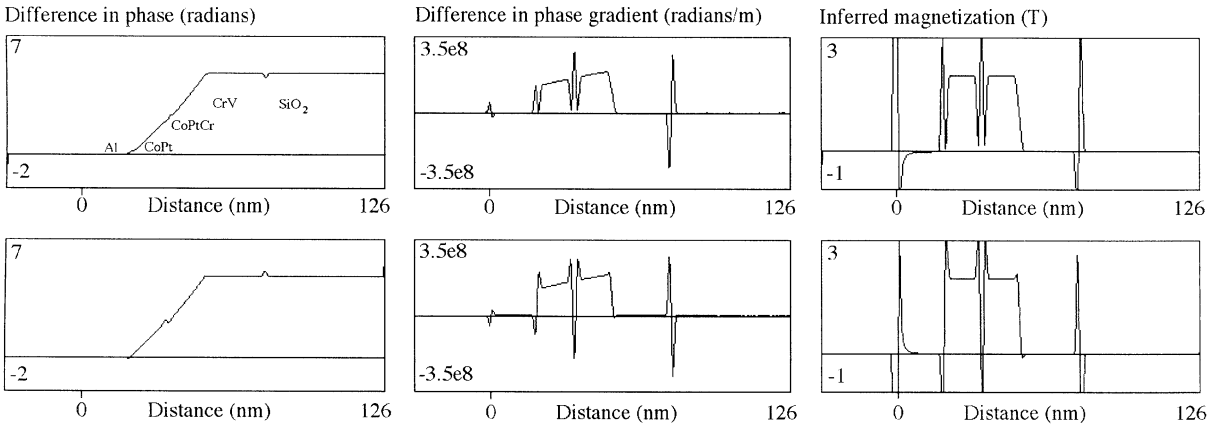

Fig. 11. Effect of small misalignment on difference between phases, difference between phase gradients and inferred magnetization using simulated phases shown in Fig. 5. Displacements are -1 (top row) and $+1$ (bottom row) pixels of effective size 0.1 nm.

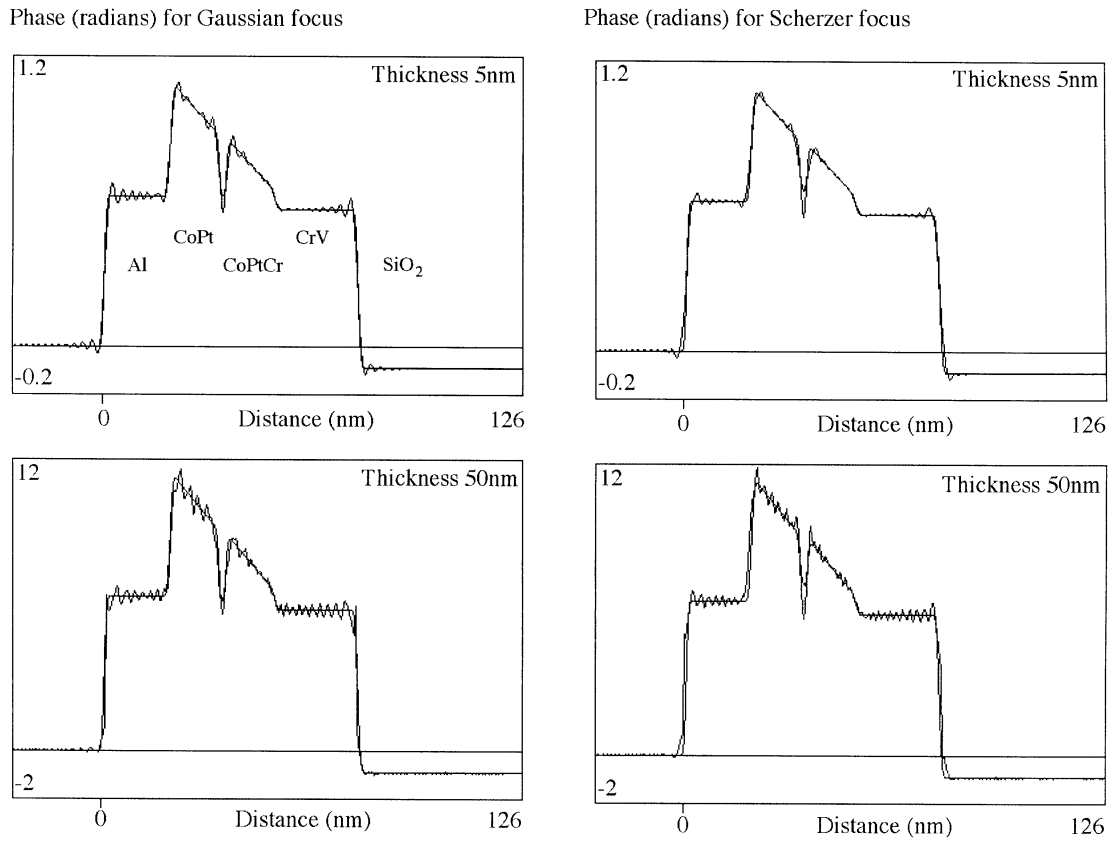

Fig. 12. One-dimensional multislice calculations of phase of cross-sectional sample, for uniform specimen thicknesses of 5 and 50 nm and defoci of 0 nm (Gaussian focus) and -4479 nm (Scherzer focus). Magnetic and mean inner potential contributions to phase change have been included. Calculations were performed for microscope parameters of 200 kV and $C_S = 8$ m, beam convergence was not included, and slice thickness and sampling density were 0.1 nm and 0.2 nm/pixel, respectively.

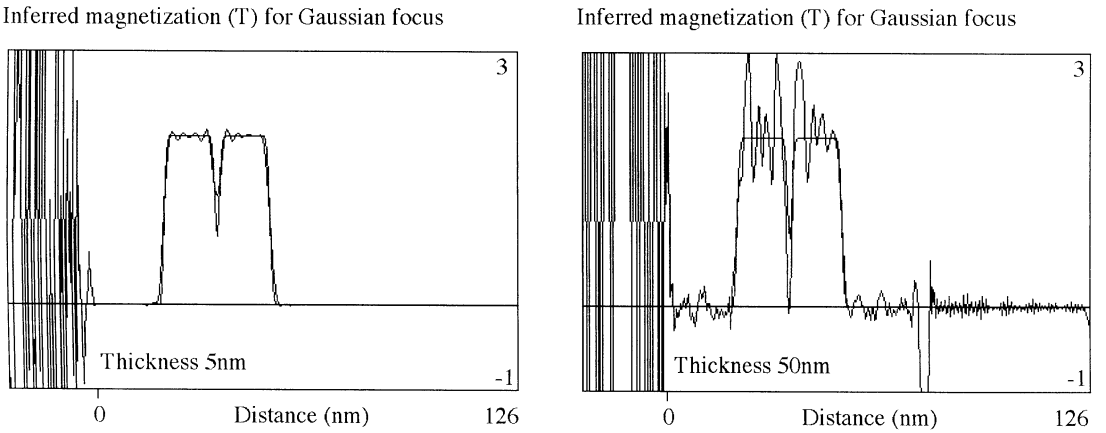

Fig. 13. Magnetization inferred from Gaussian focus profiles shown in Fig. 12 after smoothing phases using Gaussian of full-width at half-maximum 0.8 nm, displayed on top of true magnetization profiles included in original simulations. Note similarity of 50 nm simulation to Fig. 8d.

shows a comparison of the "true" magnetization profiles included in the simulations with those inferred after smoothing the Gaussian focus profiles in Fig. 12 using a Gaussian of full-width 0.8 nm. The Fresnel contrast effects are now minimal for the lower specimen thickness of 5 nm. Although they are still present for the larger thickness of 50 nm, they will be reduced further for specimens containing wider layers or less abrupt changes in composition. Further work is now required to assess the effects of Fresnel contrast for a range of specimen thicknesses.

5. Conclusions

An approach based on off-axis electron holography has been developed for characterizing the in-plane magnetization within a sample of unknown thickness that may contain both magnetic and non-magnetic regions. The approach relies on the use of the magnetic field of the objective lens to reverse the magnetization direction in the area of interest. The viability of using such in situ magnetization reversal to provide quantitative measurements of the magnetization has been demonstrated. The magnetic interactions associated with a lithographically patterned cobalt film on a silicon nitride membrane have been investigated, and an approach for characterizing the magnetization in a cross-sectional magnetic thin film or multilayer of unknown thickness has been presented. Specimen geometries such as these ensure uniform in-plane magnetization. It should be noted that our approach will not work for specimen geometries where the local magnetization in the area of interest cannot be fully reversed. Further work is now required to assess the experimental limitations imposed by dynamical contributions to the phase of the hologram.

Acknowledgements

The authors are grateful to Dr. B. Kardynal for lithographic patterning of the cobalt sample. This work was partially supported by an IBM subcontract on the DARPA Advanced MRAM Project and Contract No. MDA-972-96C-0014.

References

[1] A. Tonomura, Adv. Phys. 41 (1992) 59.
[2] J.N. Chapman, G.R. Morrison, J. Magn. Magn. Mater. 35 (1983) 254.
[3] A.C. Daykin, A.K. Petford-Long, Ultramicroscopy 58 (1995) 365.
[4] J. Dooley, M. De Graef, Ultramicroscopy 67 (1997) 13.

[5] M.R. McCartney, P. Kruit, A.H. Buist, M.R. Scheinfein, Ultramicroscopy 65 (1996) 179.
[6] M. Mankos, J.M. Cowley, M.R. Scheinfein, Phys. Stat. Sol. A 154 (1996) 469.
[7] A. Tonomura, T. Matsuda, J. Endo, T. Arii, K. Mihama, Appl. Phys. Lett. 42 (1983) 746.
[8] G. Matteucci, G.F. Missiroli, G. Pozzi, J. Electron Microscopy 45 (1996) 27.
[9] S.S.P. Parkin, Ann. Rev. Mater. Sci. 25 (1995) 357.
[10] C. Beeli, B. Doudin, J.-Ph. Ansermet, P.A. Stadelmann, Ultramicroscopy 67 (1997) 143.
[11] W.J. de Ruijter, J.K. Weiss, Ultramicroscopy 50 (1993) 269.
[12] M. Mankos, P. de Haan, V. Kambersky, G. Matteucci, M.R. McCartney, Z. Yang, M.R. Scheinfein, J.M. Cowley, in: A. Tonomura, L.F. Allard, G. Pozzi, D.C. Joy, Y.A. Ono (Eds.), Electron Holography, Elsevier, Amsterdam, 1995.
[13] W.J. Gallagher, S.S.P. Parkin, Y. Lu, X.P. Bian, A. Marley, K.P. Roche, R.A. Altman, S.A. Rishton, C. Jahnes, T.M. Shaw, G. Xiao, J. Appl. Phys. 81 (1997) 3741.
[14] Y. Lu, R.A. Altman, A. Marley, S.A. Rishton, P.L. Trouillard, G. Xiao, W.J. Gallagher, S.S.P. Parkin, Appl. Phys. Lett. 70 (1997) 2610.
[15] S. McVitie, J.N. Chapman, Microsc. Microstruct. Microanal. 3 (1997) 146.
[16] K.J. Kirk, J.N. Chapman, C.D.W. Wilkinson, Appl. Phys. Lett. 71 (1997) 539.
[17] D. Rez, P. Rez, I. Grant, Acta Crystallogr. A 50 (1994) 481.
[18] D. Jiles, Introduction to Magnetism and Magnetic Materials, Chapman & Hall, London, 1991, p. 134.
[19] R.E. Dunin-Borkowski, M.R. McCartney, B. Kardynal, David J. Smith, J. Appl. Phys. (1998), in press.
[20] M.R. McCartney, M. Gajdardziska-Josifovska, Ultramicroscopy 53 (1994) 283.
[21] G. Matteucci, M. Muccini, D. Cavalcoli, in: A. Tonomura, L.F. Allard, G. Pozzi, D.C. Joy, Y.A. Ono (Eds.), Electron Holography, Elsevier, Amsterdam, 1995.